Indoor heterogeneous photochemistry of molds and their contribution to HONO formation

C. Kalalian, A. Depoorter, L. Abis, S. Perrier, C. George

Indoor heterogeneous photochemistry of molds and their contribution to HONO formation

Carmen Kalalian[1], Antoine Depoorter[1], Letizia Abis[1], Sébastien Perrier[1], Christian George[1]*

[1] Univ Lyon, Université Claude Bernard Lyon 1, CNRS, IRCELYON, F-69626, Villeurbanne, France.

Abstract

To better understand the impact of molds on indoor air quality, we studied the photochemistry of microbial films made by *Aspergillus niger* species, a common indoor mold. Specifically, we investigated their implication in the conversion of adsorbed nitrate anions into gaseous nitrous acid (HONO) and nitrogen oxides (NO_x), as well as the related VOC emissions under different indoor conditions, using a high-resolution proton transfer reaction-time of flight-mass spectrometer (PTR-TOF-MS) and a long path absorption photometer (LOPAP). The different mold preparations were characterized by the means of direct injection into an Orbitrap high-resolution mass spectrometer with a heated electrospray ionization (ESI-Orbitrap-MS). The formation of a wide range of VOCs, having emission profiles sensitive to the types of films (either doped by potassium nitrate or not), cultivation time, UV-light irradiation, potassium nitrate concentration and relative humidity was observed. The formation of nitrous acid from these films was also determined and found to be dependent on light and relative humidity. Finally, the reaction paths for the NO_x and HONO production are proposed. This work helps to better understand the implication of microbial surfaces as a new indoor source for HONO emission.

Keywords: Microbial surfaces, Aspergillus niger, photochemistry, VOC, nitrous acid (HONO), indoor air quality

* **Corresponding author:** Christian George: christian.george@ircelyon.univ-lyon1.fr

Practical Implication

- Microbial surfaces are ubiquitous in sick buildings. They are involved in the indoor emission of spores, fragments, microbial VOCs and HONO.
- The photochemistry of microbial films doped with potassium nitrate enhances the formation of HONO.
- Indoor heterogeneous photochemistry of molds influences the indoor oxidative capacity.

1. Introduction

The health risk due to exposure to various types of indoor pollutants becomes greater as people spend exceedingly their time indoors.[1,2] Variety of pollutants might be emitted directly from indoor sources, from secondary chemistry initiated by oxidants and surface reactions or via infiltration of outdoor air.[3,4] The high surface to volume ratio (1 to 4 m^{-1})[5–8] in indoor environments points to the importance of heterogeneous chemistry through mechanisms including adsorption, oxidation reactions and acid-base chemistry.[9,10] Indoor surfaces involving different types of building materials like gypsum board, paint, glass, wood, tile, laminate, carpet, and fabric as well as furniture, human activities, and microbial activity, can be important sources and sinks of reactive pollutants indoors.[8] Volatile Organic Compounds (VOCs) are among these pollutants. VOCs can react with the indoor oxidants (like ozone (O_3) and OH radicals), resulting in the formation of multifunctional compounds in the gas phase, and can contribute to the formation of secondary organic aerosol.[8,11] VOCs are often detected indoors with higher concentrations than in the outdoor environment,[8,12,13] and their emissions depend on various environmental factors such as light, relative humidity and temperature.[9,14] However, indoor VOCs concentrations are mainly controlled by air ventilation, human occupancy and activity, alongside their indoor chemical reactions with indoor oxidants.[9,15]

In addition, growing molds in damp dwellings can be an indoor source of spores, fragments and microbial VOCs (mVOCs).[16] The most common molds identified in indoor environments are *Penicillium, Aspergillus* and *Cladosporium*.[17,18] The growth of these fungi on different surfaces is accelerated by the adequate presence of nutrients, temperature, pH and relative humidity.[15] In an indoor environment with moisture and/or high humidity, fungal spores can stick to a wide variety of organic and inorganic materials, which is the first step of colonial development and reproduction.[19] After their proliferation, they germinate and grow producing thousands of new spores using nutrients present on the different colonized substrates.[15] It was also demonstrated that the cell-to-cell interactions between the spores and/or hyphae are essential for the development of three-dimensional mycelial structures like biofilms.[19]

Moreover, as fungal cells might not be detected in the ambient air in the early stage of contamination, microbial VOCs (mVOCs) produced either by the microorganisms metabolism or by the VOCs processing, can then be used as tracers of fungal contamination within a dwelling.[20] One should note that the indoor concentrations of mVOCs in sick buildings range from few ng/m^3 to 1 mg/m^3.[21–24] In addition to producing chemicals indoors, some microorganisms are able to degrade chemical contaminants, like phthalates, emitted from home vinyl flooring.[24] Furthermore, previous studies have shown a positive correlation between the gases SO_2, NO_2, and CO and the airborne microorganisms. This correlation is probably due to the use of sulfate, nitrate, and carbonate (transformed from these gases) as the nutrients by the viable microbes.[25] In a recent study by Guo et al.,[26] the effect of different formaldehyde levels, a harmful indoor VOC emitted by various indoor surfaces, on indoor bacterial communities was established. This study has shown the interaction between formaldehyde levels and indoor bacteria and gave new insight for future studies on the interaction between indoor pollutants and microbial species.

Furthermore, one should note that the indoor environment contains highly reactive molecules and radicals such as ozone (O_3), nitrate (NO_3) and hydroxyl radicals (OH), nitrogen oxides (NO_X), sulfur dioxide (SO_2).[14] Hydroxyl radicals are now considered as the most important oxidant indoors. Recent measurements have shown that their concentrations can reach 10^6 molecules cm^{-3}, similar to outdoor daytime levels.[4] OH radicals were thought to be mainly produced during the ozonolysis of unsaturated VOC. Nonetheless, recent studies showed that the photolysis of nitrous acid (HONO), at wavelengths lower than 400 nm, can also be a source of OH radicals, contributing to more than 50% of their emissions.[4,27–30] Meanwhile, HONO can result from different sources such as combustion processes, gas-phase reactions between OH and NO, or (photo)chemical heterogeneous reactions.[1,28,31–34] The measured HONO concentrations indoors are typical around a few ppb, reaching higher values in poorly ventilated residences with gas-fired stoves.[28,29] It can also form carcinogenic nitrosamines via its reaction with secondary amines.[28] Several studies have shown that the HONO formation can be enhanced by light (300 nm< λ <400 nm).[7,27,28,32,35] Besides, nitrate anions can result from the oxidation of NO_x into nitric acid (HNO_3). Arata *et al.* performed direct measurements of N_2O_5 and NO_3 indoors, where these species react to produce HNO_3.[36] Nitric acid is likely to deposit onto surfaces, where the presence of water layers could lead to its hydrolysis and thus to the production of surface nitrate.[7] Schwartz-Narbonne et al. characterized real indoor films (collected from the living room and kitchen) in terms of water uptake and ionic composition and found concentrations of nitrate anion ranging from 7.57 to 25.17 $\mu g/cm^2$.[9] Liu et al.[37] have also identified different anions (F^-, Cl^-, Br^-, NO_3^-, PO_4^{3-}, SO_4^{2-}) on glass plates collected from the kitchen with concentrations from 0.117 to 142.499 ppm.

Indoor surfaces are typically covered by a complex mix of organic and inorganic compounds.[9,32,38,39] In this work, we investigated the photochemistry of microbial films made by *Aspergillus niger* species, a common indoor mold, and their implication in the conversion of

adsorbed nitrate anions into gaseous nitrous acid, nitrogen oxides, and associated VOC emissions, as a function of light irradiation, relative humidity and molds cultivation time. This will unravel the implication of microbial surfaces, ubiquitous in sick buildings, in the HONO formation, affecting the indoors oxidative capacity and will help better understand interactions between microbes and chemistry in human-dominated habitation.

2. Experimental section

2.1.Molds and film preparations

Molds were cultivated on a synthetic malt agar extract, recommended for the cultivation of indoor mold species.[40] The protocols used for the culture medium preparation, as well as the species identification by molecular biology are described by Kalalian et al. [23] The grown molds belonged to the *Aspergillus sp.* type *Aspergillus niger***.**

The first step of the film preparation was to wash a grown molds' petri dish with Milli-Q water (18.2 MΩ cm), in order to create a solution, named "molds extract", containing a suspension of molds in water. Then, the second step consisted in filling a petri dish (40 mm in diameter) with either (i) a solution of molds extract or (ii) a solution of potassium nitrate KNO_3 and (iii) a mixed solution of molds extract and potassium nitrate KNO_3. The concentrations of the potassium nitrate KNO_3 solutions were varied from 0.001 M to 0.5 M. The preparations were dried over a period of 12 hours in an oven at 323.2 ± 0.1 K. Once dried, the petri dishes were weighed again (the empty petri dishes were weighed beforehand) and used directly (within one day) in the planned experiments.

2.2.Experimental setup

Experiments were performed in an 80 cm^3 borosilicate reactor under a constant flow of dry/humid synthetic air, or synthetic N_2, and irradiated from the top by a 340 nm LED lamp (ThorLabs, 60mW, nominal maximum irradiance of 2.22 W/m^2). The humidity in the reactor

was varied by changing the mixing ratio of dry or humid carrier gas. The temperature (T = 25 ± 2°C) and the relative humidity in the reactor (RH = 0-85% ± 2%) were controlled by a humidity and temperature probe (Vaisala HUMICAP® HMP110).

In this study, two different experimental systems were used as shown in **Figure S1 in the supporting materials (SM)**. Setup 1 was designed for VOC analysis, where the reactor was coupled to a high-resolution proton transfer reaction-time of flight-mass spectrometer (PTR-TOF-MS) and flushed by 120 mL/min of air (or N_2). For this setup (setup 1), a measurement cycle consisted of measuring the VOC concentrations at the outlet of the reactor containing the film for 5 min, then the LED lamp was switched on for 15 min. In contrast, the second approach was designed to measure NO_X and HONO formation. For setup 2, the reactor was coupled to a NO_X analyzer and a Long Path Absorption Photometer (LOPAP) and flushed by 500 mL/min of synthetic air (or N_2). The irradiation time was around 60 min.

Nonetheless, prior to each experiment, a blank control involving sterile petri dishes was performed under the same experimental conditions.

2.3. Analytical tools

2.3.1. UV- visible analysis

The UV-visible spectra of initial solutions, as well as extracted films of molds, potassium nitrate and mix film of molds and potassium nitrate, were determined in the range of 200–600 nm using a Cary 60 UV-Vis spectrophotometer from Agilent Technologies. Films were extracted with 2 mL of Milli-Q water and diluted from 2 to 20 times. Samples were then placed within a 3500 µL Macro Fluorescence Cuvette (Thorlabs) to perform the measurement. Three replicas were performed for each type of extracted film or solution.

2.3.2. Mass spectrometry analysis

It was demonstrated by Depoorter et al. [32] that a possible reaction may occur between nitrate anions and reactive organic compounds during the drying process of a wet film, resulting in the formation of nitro groups. Therefore, we characterized the potential formation of nitrogenated compounds in a mixed solution of molds extract and potassium nitrate using a direct infusion in an Orbitrap high-resolution mass spectrometer (HRMS, Q Exactive, Thermo Scientific, Bremen, Germany) with a heated electrospray ionization (ESI). These results were compared to different blanks using water, molds extract solution and potassium nitrate solution, respectively. It is noteworthy to mention that the solutions were filtered through a 0.2 µm Hydrophilic Polypropylene membrane (GHP,13 mm, Pall Corporation, USA).

Samples were injected into the MS through a steel capillary by a Hamilton syringe of 500 µL (SGE Analytical Science) at a flow rate of 10 µL/min and were analyzed using a spray voltage of −4 kV and +4 KV for negative and positive ionization mode (ESI− and ESI+) measurements, respectively. The temperature of the Orbitrap capillary was set at 250°C. The system was operated in both ESI+ and ESI- mode with a resolving mass power of 140 000 at m/z 200. A sodium acetate solution (2 mM in 50/50, v/v, ACN/water) was used for the mass calibration; this solution provides a series of negative and positive adduct ions in the scanning range of m/z 50–750.[41,42] The calibration method consisted in filling the syringe with a 2 mM solution of sodium acetate and setting the syringe pump flow rate to 20 µL/min. Once the calibration started, few minutes wait are needed for a stable system with a stable TIC (deviation <10%). The accuracy of the calibration is then evaluated (lower than 0.5 ppm). This procedure is made for both modes (positive and negative). Signals in the range of m/z from 50 to 750 were then recorded and processed for formula calculations.

Data were processed and evaluated using Xcalibur 2.2 (Thermo, USA). The subsequent non-target screening approach was conducted using MZmine 2.53 software.[41,42] This software

provides the main functionality for MS data processing: raw data import, mass detection, chromatogram building, deisotoping, alignment, identification, and duplicate peak filtering. The detailed processing steps and settings can be found in Wang et al.[42] and in Table S1. Molecular formulas tentatively identified were expressed as $C_cH_hO_oN_nS_s$, where c, h, o, n, and s correspond to the numbers of carbon, hydrogen, oxygen, nitrogen, and sulfur atoms in the molecular formula, respectively. Molecular formulas were assigned to detected signals satisfying the following constraints: 1−50 for ^{12}C, 1−50 for ^{1}H, 0− 40 for ^{16}O, 0−10 for ^{14}N, 0−3 for ^{32}S, 0−1 for ^{13}C, 0−1 for ^{18}O, and 0−1 for ^{34}S. The mass tolerance was 2 ppm for ESI− and 3 ppm for ESI+. Several rules were also considered: H/C ratio, $0.3 \leq H/C \leq 3$; NOPS/C ratios, $N/C \leq 2$, $O/C \leq 2$, $S/C \leq 2$. In the positive mode, 0−2 of ^{23}Na was also included in the formula calculation because of the high tendency of Na to form adducts with polar organic molecules.[43] The ring and double bond equivalence ($RDBE$) value was calculated as follow:

$$RDBE = \frac{2\times C+2+N-H}{2} \qquad \textbf{(Eq. 1)}$$

The $RDBE$ values considered in this study were in the range of 0–25. However, $RDBE$ may not accurately indicate the level of unsaturation for compounds with heteroatoms (e.g., O, N, and S). For this reason, the aromaticity equivalent (X_c) was also calculated. A threshold values for X_c were proposed in the literature, where $X_c \geq 2.5$ and $X_c \geq 2.7143$ are the unambiguous minimum criterion for the presence of aromatic and condensed aromatic structures in a molecule, respectively.[44] X_c for compounds containing carbon, hydrogen, nitrogen, oxygen, sulfur, and phosphorus can be calculated as follow:

$$X_c = \frac{3\times(RDBE-(p\times O+q\times S))-2}{RDBE-(p\times O+q\times S)} \qquad \textbf{(Eq. 2)}$$

where p and q correspond to the fraction of oxygen and sulfur atoms involved in π-bond structures of a compound, respectively. $p = q = 1$ for aldehydes, ketones, nitroso and cyanate compounds, $p = q = 0.5$ for carboxylic acid, ester and nitro compounds, and $p = q = 0$ for

alcohols, ethers and peroxides.[44]

Aligned peak lists from MZmine workflow and xcalibur were further processed with three different databases Swiss-Prot,[45] metabolomics workbench,[46] and the protein data bank [47] to ensure the most relevant tentatively identified formulas. Only peaks with intensities at least 10-100 times higher than the mentioned blanks were considered to check the possible formation of nitrogenated compounds.

2.3.3. HONO and NO_X measurements

A long path absorption photometer (LOPAP, QUMA) was used to measure the concentration of gaseous nitrous acid. For such measurements, HONO is sampled in a glass stripping coil by a fast-chemical reaction and converted into an azo dye which is photometrically detected in long path absorption inside a special Teflon tubing (Teflon AF2400). During the experiments, the integrated time resolution was 7 minutes, and the detection limit was less than 10 pptv under our operating conditions (inlet gas flow set to 500 mL/min and liquid flow of the reagents set to 20 mL/min). The sampling unit was maintained at 293 ± 0.02 K, using a Thermo Scientific ARCTIC Refrigerated/Heated Bath (SC100 A10 - 230V). In addition, one should note that the instrument was calibrated each week. The full description of this device is detailed elsewhere.[48,49]Furthermore, a chemiluminescence NO_X analyzer (CLD 88 CY analyzer, Eco Physics) was used to measure the NO and NO_2 concentrations, with a detection limit of 50 ppt. Prior to a series of measurements, the NO_x analyzer was calibrated. the calibration consisted of doing a zero point of the instrument using a nitrogen/air flow and then doing a span point with a known NO concentration. Then, to check the linearity of the instrument in the working range, calibration curves for NO (~1 ppm in N_2, Linde) and NO_2 (850 ppb in N_2, Linde) in the range 0-100 ppb were established.

2.3.4. VOC analysis

VOCs released by the films were continuously analyzed using a high-resolution proton transfer reaction-time of flight-mass spectrometer (PTR-TOF-MS 8000, Ionicon Analytik). The ionization was carried out in the H_3O^+ mode. This instrument allows the estimation of the VOC concentrations without an external calibration[50] and its full description can be found elsewhere.[50,51] For all the experiments, the instrument settings were chosen as follows: drift tube voltage at 500 V, drift tube temperature at 353 K with a drift pressure of 2.2 mbar. The E/N ratio was 125 Td where 1 Td = 10^{-17} V cm^2. Furthermore, in order to reduce the adsorption and the products loss, the reactor's outlet and the PTR-TOF-MS sample inlet tubing were constantly heated at 333 K. All the spectra were recorded with a time resolution of 1 s and a mass resolution of 4500 m/Δm. A calibration gas standard containing 14 VOCs with a concentration of 100 ± 10 ppb in nitrogen (TO-14A Aromatic Mix, Restek Corporation, Bellefonte, USA) was used to control the instrument performance in terms of mass resolution, mass accuracy, sensitivity, and relative mass-dependent transmission efficiency.

TofViewer v1.4.3 software was used for raw spectral data analysis, mass calibration, peak fitting, and area extraction. The mass calibration was performed using internal calibration based on two references ions with an exactly known mass (i) hydronium ion isotope ($H_3{}^{18}O^+$ m/z 21.022) and (ii) protonated acetone ($C_3H_7O^+$ m/z 59.049).[52,53] The used protonation reaction rate constant was 2×10^{-9} cm^3 s^{-1} for all the detected masses. Conjointly, the VOC concentrations were calculated according to the equation given by Cappellin et al.,[50] where the uncertainties on the absolute concentrations can be estimated to be about 30-40 % arising from systematic errors. Furthermore, as the variation of relative humidity in the sampled air can affect the H_3O^+ and $H_3O^+(H_2O)$ ions signals and thus the H_3O^+ to $H_3O^+(H_2O)$ ratio, the VOC ion signals were normalized to a standard reagent ion signal of 10^6 counts s^{-1} (cps) according to the procedure given by de Gouw et al. [51]

The collected experimental dataset contains around 160 variables corresponding to the number of peaks detected in PTR-TOF-MS measurements. In order to evaluate the effect of the different tested conditions of relative humidity, cultivation time, type of films and potassium nitrate concentrations on the VOC emission profiles, the principal component analysis (PCA, package FactormineR, Ade4 Version 1.0.153–©2009-2017 R Studio) was performed on the datasets using R software (Version 1.0.153 – ©2009–2017 RStudio). The PCA allows a statistical representation of all data without any preconception as to the type of emitted compounds and without bias. PCA can generate optimum and similar graphical representations of the scatterplot representing the data matrix. Each PCA factor is a linear combination of variables representing the maximum variance in the scatterplot. As the factors have an orthogonal relationship, only independent sources of variance are taken into account.[54]

2.3.5. Reagents

Potassium nitrate (99%), sodium acetate (≥99 %), and lactic acid (90%) were purchased from Sigma Aldrich. Malt agar extract was provided by Biokar diagnostics. The air (>99.9%) and dinitrogen N_2 (>99.9992%) were either synthetic or obtained from Air Products. NO (~1 ppm in N_2) and NO_2 (850 ppb in N_2) were provides by Linde.

3. Results and discussion

3.1.Film characterization

The UV analyses were performed on three types of films (molds, KNO_3 and mix of molds and KNO_3) extracted with milli-Q water and were compared to their initial corresponding solutions. Both solutions and extracted films showed similar trends **(Figure S2 in the SM)**. For the KNO_3 extracted films, a band centered at 300 nm was observed consistent with the literature.[55] For the molds extracted films, the UV spectrum shows a band with three large peaks: at 313 nm, 285 nm and 247 nm, which could be a combination of different compounds exhibiting various

functional groups and conjugations. As for the mixed extracted film of molds and potassium nitrate, a band centered at 292 nm was observed. It was however not possible to assign a functional group for this band. In fact, the presence of organic compounds (molds extract in this study) modifies the molecular structure of adsorbed nitrate anions, and leads to a red shift in the actinic region, which can increase the light absorbed by nitrate anions.[56] Moreover, to check if the mixing time of the molds extract and potassium nitrate affects its UV spectrum, the UV spectrum of a mixed solution was recorded at different times after mixing i.e., 3 and 12 hours of mixing (same time used for the film preparation) and the results are presented in **Figure S3 in the SM**. These results show that the mixing time did not affect the UV spectrum of the mixed solution of molds extract and potassium nitrate.

Spectral analysis of irradiated films of molds, KNO_3 and mix of molds and KNO_3 by the LED at 340 nm revealed a change in the shape of the bands i.e., mainly a decrease in intensity suggesting a possible degradation of the films upon irradiation **(Figure S4 in the SM)**.

The MS analysis allowed the identification of 7 molecular formulas only in ESI+ that are exclusively present in the mix solution of molds extract and potassium nitrate. **Table 1** summarizes the detected masses in ESI+ with the tentatively identified formulas, $RDBE$, X_c, potential origin and the ratios H/C, O/C, N/C, S/C, N/O. Moreover, O/N ratios were determined for each of the tentative compounds, in the range from 0.5 to 7. O/N ratios larger than 3 points toward the presence of a nitro ($-NO_2$) function to the proposed formulas. However, formulas with O/N ≤ 1 could contain a reduced nitrogen functions, such as amines and amides.[42,43] These compounds have high H/C ratios compared to O/C ones. Formulas with 1 ≤ O/N ≤ 3 could be a combination of different functional groups like nitramines ($N-NO_2$). Therefore, the detected molecules are mainly amino acids, nucleic acid, peptide and dipeptide fragments, membrane fractions and metabolites. Most of the tentatively identified formulas possesses a nitro group (-

291 NO_2), possibly related to a nitration reaction during the preparation of the mix solution of molds
292 extract and potassium nitrate.

293 As demonstrated in previous studies, protein nitration can occur in the gas phase in the
294 presence of nitrogen dioxide (NO_2) and ozone (O_3).[57,58] However, as proposed by Ghiani et
295 al.,[59] the protein nitration can also take place in the aqueous phase in the presence of nitrate ions
296 (NO_3^-) with concentrations and pH levels comparable to that found in the aerosol liquid water
297 phase both in the dark and under UV-A irradiation. The nitration of aromatic compounds, such
298 as phenols, can occur both in the gas phase in the presence of OH and NO_2 or NO_3 and NO_2,
299 and by multiphase various reactions involving nitrogen dioxide, N_2O_5 and/or $ClNO_2$, NO_3,
300 nitrate or nitrite when irradiated. Nitration is also induced by the presence of dissolved Fe(III),
301 nitrate, semiconductor oxides.[60] Additionally, HNO_2 may react in the dark with hydrogen
302 peroxide to form peroxynitrous acid (HOONO), allowing consequently the oxidation and
303 nitration of aromatic compounds.[60]

304 On the other hand, it is well known that *Aspergillus sp* can use a broad range of nitrogen
305 sources, such as ammonium, nitrate, amino acids (e.g., histidine or proline), or complex
306 substrates such as collagen and elastin. The nitrate assimilation by fungi leads to the complete
307 reduction of nitrate forming ammonium, which is finally incorporated in the amino acids
308 glutamate and glutamine acting as nitrogen donors.[61] Moreover, fungi can also synthesize NO
309 from nitrate through the action of nitrate reductase.[62] In the presence of superoxide (O_2^-),
310 peroxynitrite (ONO_2^-) can be formed and cause protein modification, lipid oxidation, and DNA
311 damage.[63,64] It was further demonstrated that peroxynitrite can nitrate and oxidize tyrosine
312 residues in membrane proteins and can cause as well lipid oxidation and nitration.[63,65,66]

313 For all the reasons cited above, we hypothesized that a combination of biotic and abiotic
314 factors might have contributed to the formation of the nitro compounds that were observed in
315 our study.

316 **Table 1:** Potential identities and sources for the identified compounds from a mixed solution of molds extract and potassium nitrate in ESI+ mass
317 spectra.

Detected Masses (Da)	Neutral mass (Da)	Possible Formula	Possible identity	Potential origin	H/C	O/C	N/C	S/C	O/N	RDBE	Xc (p=q=1)	Xc (p=q=0.5)
219.14902	218.14902	$C_{13}H_{18}N_2O$	5-Methoxydimethyltryptamine	Tryptamine derivatives	1.4	0.1	0.2	0.0	0.5	6.0	2.60	2.64
223.18029	222.18029	$C_{13}H_{22}N_2O$	Nigragillin	Alkaloid - metabolites from the *A.niger*	1.7	0.1	0.2	0.0	0.5	4.0	2.33	2.43
246.01611	223.01611	$C_5H_9N_3O_5S$	N-nitro-L-cysteinyl-glycine (NO_2-Cys-Gly-OH)	Peptide L-cys-gly	1.8	1.0	0.6	0.2	1.7	3.0	3.67	0.00
		$C_{13}H_5NO_3$	Possible nitro	NI	0.4	0.2	0.1	0.0	3.0	12.0	2.78	2.81
260.03182	237.03182	$C_{14}H_7NO_3$	1-ethynyl-7-nitrodibenzofuran / 3-nitro-15-oxatetracyclo[10.2.1.05,14.08,13]pentadeca-1(14),2,4,6,8(13),9,11-heptaene	Miscellenious compound *a.niger* / n-myristoyltransferase	0.5	0.2	0.1	0.0	3.0	12.0	2.78	2.81
		$C_5H_8N_4O_7$	4,5-dimethoxy-1,3-dinitroimidazolidin-2-one / N-methyl-4,4,4-trinitrobutanamide	Imidazolinone /Amino acids or dipeptides: glutamine or beta-Ala-Gly	1.6	1.4	0.8	0.0	1.8	4.0	3.67	1.00
	259.03182	$C_{11}H_6N_4O_2S$	3-nitro-4-pyrimidin-2-ylsulfanylbenzonitrile / 3,6-bis(2-furanyl)-[1,2,4]triazolo[3,4-b][1,3,4]thiadiazole	Nucleic acid derivatives	0.5	0.2	0.4	0.1	0.5	11.0	2.75	2.79
262.01109	239.01109	$C_{13}H_5NO_4$	Possible nitro	NI	0.4	0.3	0.1	0.0	4.0	12.0	2.75	2.80
		$C_4H_6N_4O_8$	Tetranitrobutane	Protein hydrolase/toxin n-butane	1.5	2.0	1.0	0.0	2.0	4.0	3.50	0.00

		$C_3H_4N_6O_7$	1,3,5-Trinitro-1,3,5-triazinan-2-one	Triazine moity-amino acids:peptides	1.3	2.3	2.0	0.0	1.2	5.0	4.00	1.67
263.01442	240.01442	$C_{13}H_5NO_4$	Possible nitro	NI	0.4	0.3	0.1	0.0	4.0	12.0	2.75	2.80
	262.01442	$C_6H_4N_4O_8$	5-Amino-2,4,6-trinitro-1,3-benzenediol	2,6-dihydroxyaniline/N-ethylmaleimide	0.7	1.3	0.7	0.0	2.0	7.0	5.00	2.33
264.00919	241.00919	$C_{13}H_7NO_2S$	2-nitro-9H-fluorene-9-thione	Fluorene/membrane fraction fatty acyls	0.5	0.2	0.1	0.1	2.0	11.0	2.75	2.79
	219.00919	$C_7H_9NO_7$	6-Methoxy-5-nitro-4,6-dioxohexanoic acid	Skikimic acid (intermediate metabolites microorganism)	1.3	1.0	0.1	0.0	7.0	4.0	3.67	1.00

NI: not identified

3.2. VOC emission from films

The VOC emissions from molds films, either mixed or not with KNO_3, were investigated for different molds cultivation time, under different relative humidities, under dark and irradiation conditions, under N_2 and air streams, and for different concentrations of KNO_3 (0.001-0.5M). In this section, only the results for the effect of KNO_3 on VOC emission profiles are presented. More details about the impact of the other cited conditions are available in the **supporting materials.**

To visualize the impact of the type of film on the VOC emission profiles, a PCA was performed and is presented in **Figure 1**. PCA_1 described 38.8 % of the total dataset variability (28.8% for the first dimension and 10% for the second one). According to **Figure 1**, each film shows a very differentiated VOC emission profile (ellipses grouping the different conditions (i.e., film type) are well separated). It is also noticeable that all the differences between the three film types are almost driven by compounds emitted by molds' films doped with potassium nitrate.

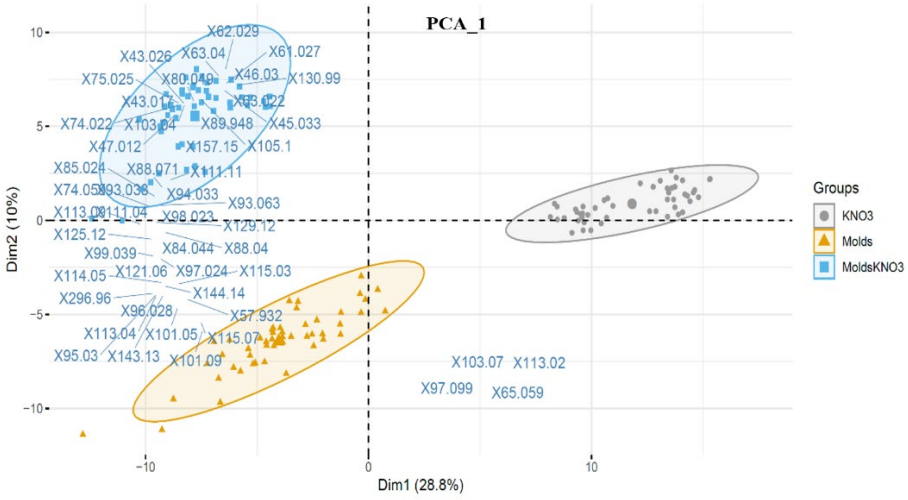

Figure 1 :VOC emission profiles at RH = 85% for different types of films: molds, KNO_3 and molds + KNO_3. The molds were incubated for 10 days and [KNO_3] = 0.04M. The m/z of the 50 compounds that are most explaining the variance in the two first components are presented on the graph. The percentages of the eigenvalues of the two first components are shown on each axis.

Furthermore, in order to determine the effect of the potassium nitrate concentration on the VOC emission profiles, another PCA (PCA_2) was performed on the dataset (**Figure 2-a**) and the relative abundance of each VOC detected from molds films doped with different concentrations of potassium nitrate were determined and compared in **Figure 2-b**. PCA_2 described 22 % of the total dataset variability (17.5% for the first dimension and 4.5% for the second one). The ellipses grouping the different conditions (KNO_3 concentrations) are separated with an overlap between the film with higher potassium nitrate concentration (0.04M, 0.1M and 0.5M). It is also noticeable that 42 of the 50 compounds are driven by the films with higher potassium nitrate concentration, explaining the variance between the different conditions. Likewise, **Figure 2-b** shows variability in the VOC emission profiles, which is in line with the results obtained by PCA_1 and PCA_2 analyses. Hence, according to **Figures 1 and 2**, the presence of potassium nitrate in the films affects their composition and thus their VOC emission profiles.

Nonetheless, in the absence or presence of UV-light, the concentration of some VOCs increased with the increase of potassium nitrate concentrations as shown in **Figure 2-b**. Among those VOCs: succinimide ($C_4H_5NO_2$) and butene (C_4H_8), where their relative abundances increase from 0% for [KNO_3] = 0-0.001M to 6.1% and 20.5% for [KNO_3] = 0.5M, respectively. The evolution of some VOC concentrations in response to the different potassium nitrate concentrations in the films reflects the possible interaction between the nitrate solution and the molds extract during the film preparation. As for the VOCs that are both sensitive to UV-light irradiation and potassium nitrate concentration, they might be released in the gas phase in response to the photodegradation of nitrogenated compounds that can be formed during the film preparation (**Figure 2-b and Table S2)**.

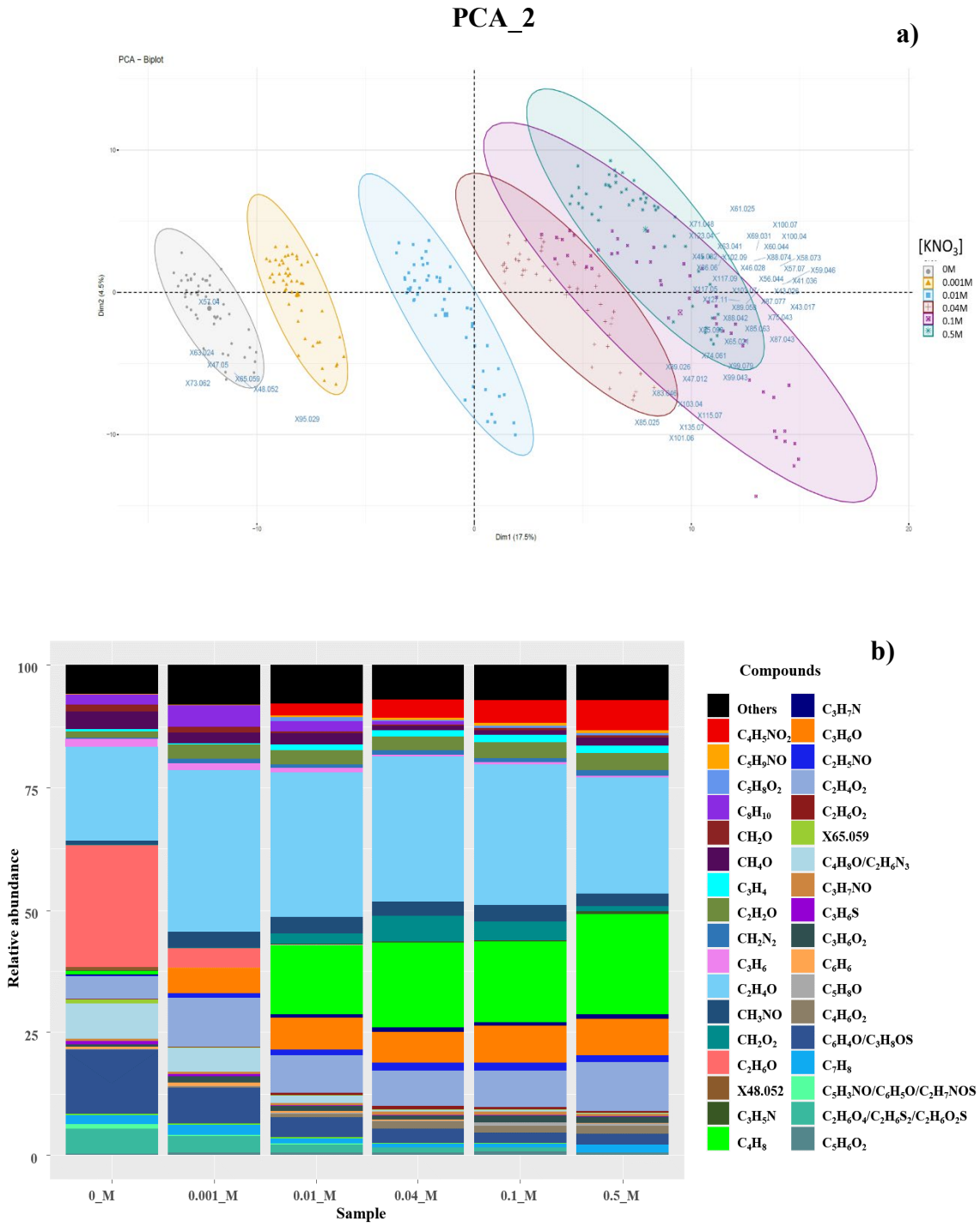

Figure 2: (a) VOC emission profiles for mold films doped with different KNO_3 concentrations. The m/z of the 50 compounds that are most explaining the variance in the two first components are presented on the graph. The percentages of the eigenvalues of the two first components are shown on each axis (b) Relative abundance of the most emitted VOCs from these films. RH=85% and molds were incubated for 14 days.

3.3.HONO and NO_x emission

The temporal evolution of HONO formation under an air stream, from the three sets of film samples (irradiated films of molds, KNO_3 and mold films doped with KNO_3) and compared to a reactor blank with a relative humidity of 85±2% is presented in **Figure 3**. The uncertainties on the concentrations were twice the standard deviation. When the LED lamp was switched ON, an enhancement of the HONO concentration was observed. The HONO concentration increases to a maximum value of 900 ppt and then stabilizes at a value of 700 ppt. It is noteworthy mentioning that the formation of HONO from irradiated mold films doped with KNO_3 was also observed under a nitrogen stream with concentrations in the same order as that under air stream. However, individually molds and nitrate films showed a negligible formation of HONO compared to a blank experiment with an empty reactor. In fact, the wavelengths of the LED lamp used in this study ranged between 335 and 380 nm. Thus, at these wavelengths, the photochemistry of potassium nitrate cannot be activated efficiently because due to a low absorption beyond 335 nm.[32]

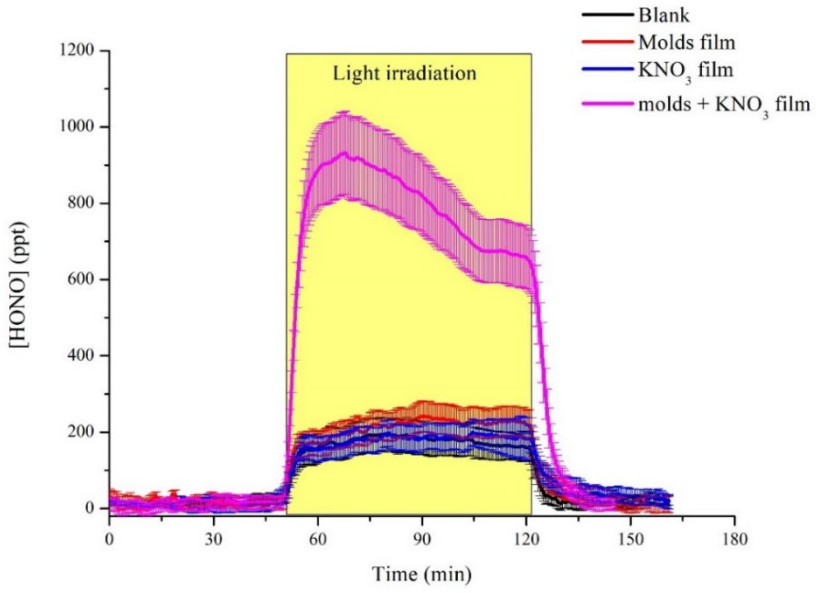

Figure 3: Formation of HONO (ppt) in response to the irradiation of molds films, KNO_3 films and molds films doped with 0.04M of KNO_3 and compared to a reactor blank. RH=85±2%, error is 2σ, yellow area corresponds to light irradiation.

Additionally, the concentration of nitrate in the film was also varied from 0.001M to 0.5M. As the KNO_3 concentration increases, a slight increase of the HONO concentration was observed in **Figure 4-a**. However, for higher concentration values of KNO_3, the formation of HONO decreased. Likewise, the proportion of nitrate and molds in the films was varied. These results show a maximum HONO formation for a stoichiometric mix of molds and nitrate in the initial solution **(Figure 4-b)** and a decrease of the HONO concentration when KNO_3 was in excess.

The decrease of the HONO concentration for high KNO_3 concentration can be explained by the fact that the gaseous products formed during the photolysis of the film may hardly escape from the nitrate crystal that is saturating the surface. A similar behavior was previously observed from mixed films of furfural and KNO_3 [32] as well as from films of humic acids and KNO_3 [39] where a decrease of the HONO formation was also witnessed for high potassium nitrate concentrations.

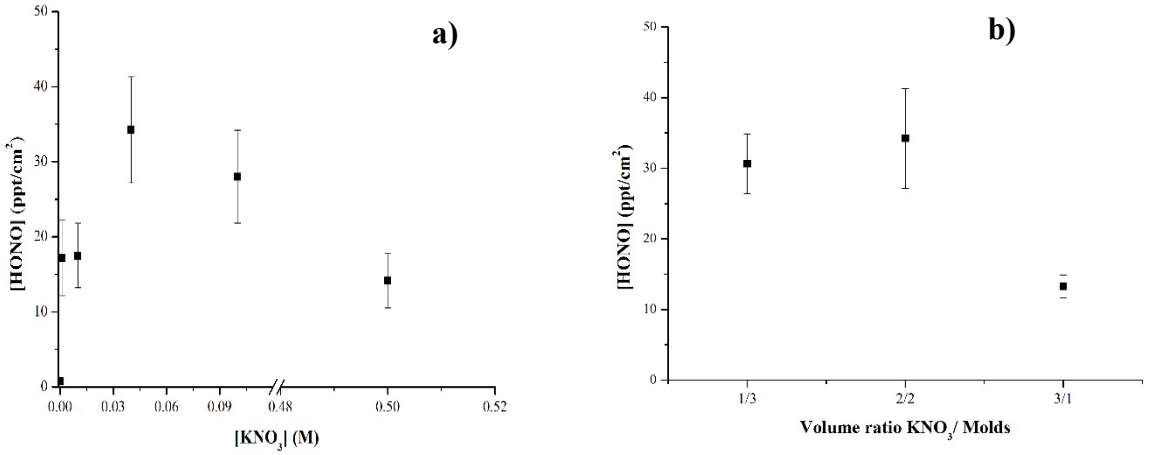

Figure 4: Variation of [HONO] (ppt/cm^2) as (a) function of [KNO_3] (M) used in the film preparation and (b) for different volume ratio KNO_3/molds. The reactor blank is subtracted and error bars correspond to 1σ.

Furthermore, to assess the effect of the relative humidity on the gas-phase formation of NO, NO_2 and HONO from mold films doped with KNO_3, different relative humidities were

tested (RH= 0-85 ±2%), and the results are shown in **Figure 5**. The maximum tested relative humidity was below the deliquescence point of potassium nitrate (>92%).[67] Each point corresponds to the average of 3-4 replicas and the error bars correspond to one standard deviation. It was found that with increasing relative humidity, both NO_2 and HONO concentrations increase. However, NO formation seemed to be less sensitive to the variation of relative humidity. Pure KNO_3 films and mold films were unable to produce HONO and NO_X.

These results show that an increased amount of HONO is generated by the photolysis of nitrates when mixed with organic matter (molds extract) with increasing relative humidity. The observed HONO formation during irradiation might also result, in part, from the photodegradation of nitro compounds (mainly nitrated proteins, amino acids or metabolites), formed during the film preparation process.

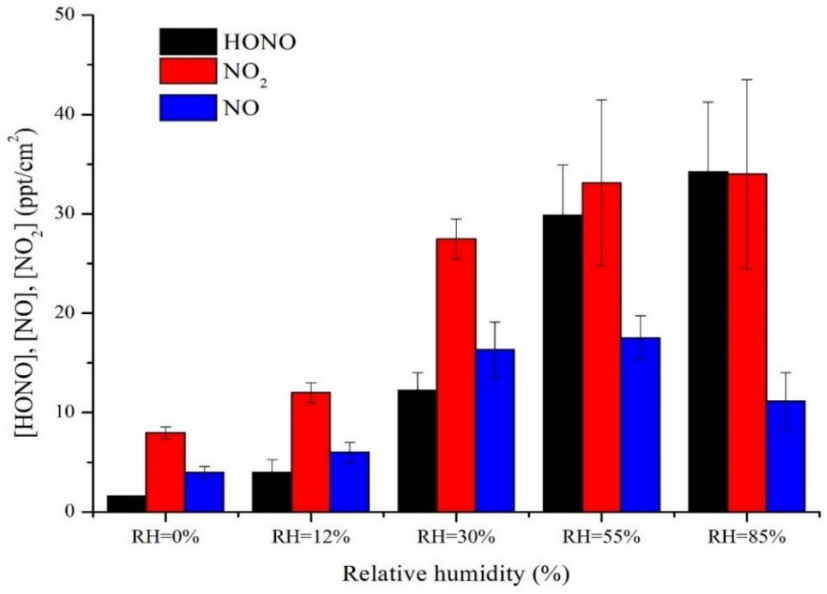

Figure 5: Variation of [HONO] and [NO_X] in ppt/cm^2 as a function of the relative humidity from mold films doped with 0.04M of KNO_3, error bars correspond to 1σ.

3.4. Reaction mechanism

Based on the results obtained in this study and that of the available literature, different routes explaining the photochemical formation of NO, NO_2 and HONO are proposed.

The mass spectrometry analysis of the mixed solution of molds extract and potassium nitrate showed the formation of some nitro and nitrogenated compounds during the film preparation. Depoorter et al.[32] have also shown a possible nitration reaction during the preparation of furfural and potassium nitrate films. The authors have proposed a mechanism for the photochemical degradation of 2-nitrofuran (a proxy for nitro compounds formed during the preparation of furfural films doped with KNO_3). The photodegradation of 2-nitrofuran results in the (i) formation of NO and $C_4H_3O_2$, (ii) formation of NO_2 and C_4H_4O, and (iii) formation of HONO following the reduction of NO_2 on surfaces containing reducing functionalities. This photodegradation can occur under both nitrogen and air streams, where the authors have probed the possible formation of O_2^- on the surface which can increase the oxidative capacity of the surfaces leading to an evolution of the concentrations of nitrogen containing compounds at the gas-surface interface. Moreover, Wang et al.[33] reported that reactions between NO_x and HO_2/O_2^- in the aerosol phase are a significant pathway by which HONO production is enhanced in the presence of dissolved aliphatic organic matter. This chemistry can be applied to many aqueous environments (e.g., cloud droplets, aqueous aerosols, and surface water) and may represent a significant source of gaseous HONO in areas where surface waters or aqueous microlayers contain a high concentration of nitrate and dissolved aliphatic organic matter.

On the other hand, the presence of molds extract as a source of organic compounds on the surface can modify the molecular structure of nitrate anions leading to a red shift into the actinic region and an enhancement of the light absorbed by nitrate anions.[56] Depending on the surface pH, nitrate can be transformed into nitric acid. In fact, among the VOC released from molds film doped with KNO_3, some acids were detected that can promote surface acidity. The photolysis of adsorbed nitric acid/ nitrate (HNO_3/$nitrate_{(ads)}$) can directly produce HONO and NO_2 via reactions R1-R3 or indirectly through reactions R4 and R5.[56,68–70] The produced NO_2 from reaction (R2) and HONO from reactions (R3, R4 and R5) are released from the surface to

454 the gas phase following reactions (R6) and (R7). The $Org_{(ads)}$ corresponds to molds extract in
455 this study.

$$HNO_3\,/nitrate_{ads} \xrightarrow{hv} [HNO_3\ /nitrate]^*_{(ads)} \quad \textbf{(R1)}$$

$$\xrightarrow{hv} NO_{2(ads)} + OH_{(ads)} \quad \textbf{(R2)}$$

$$\xrightarrow{hv} HONO_{(ads)} + O(\,^3P)_{(ads)} \quad \textbf{(R3)}$$

$$NO_{2(ads)} + H_2O_{(ads)} \xrightarrow{hv} OH_{(ads)} + HONO_{(ads)} \quad \textbf{(R4)}$$

$$NO_{2(ads)} + Org_{(ads)} \xrightarrow{hv} Org - oxidized_{(ads)} + HONO_{(ads)} \quad \textbf{(R5)}$$

$$HONO_{(ads)} \rightarrow HONO_{(g)} \quad \textbf{(R6)}$$

$$NO_{2(ads)} \rightarrow NO_{2(g)} \quad \textbf{(R7)}$$

456 Nevertheless, *Aspergillus niger* species contain Aspergillin that is classified as melanin
457 or a humic acid-containing chromophore groups.[71] Yang et al.[39] and Stemmler et al.[72] suggested
458 that the presence of chromophoric centers, like aromatic carbonyls in humic acids, could act as
459 photosensitizers in the photolysis of nitrates or in the conversion of adsorbed NO_2 into HONO.
460 Additionally, during the photolysis of nitrate and humic acids, aromatic nitro compounds are
461 expected to be formed by the photochemical oxidation of nitrates. Correspondingly, it has been
462 reported that the photolysis of nitro-aromatic compounds may lead to the HONO formation.[39]
463 Furthermore, the photolysis of species containing a nitrogen atom in humic acids may release
464 gaseous products such as HONO and NO_2.[39] And it was previously demonstrated that the
465 photolysis of ortho-nitrophenols (as is the case for 3-nitrotyrosine) can generate nitrous acid
466 (HONO).[58] Thus the photodegradation of nitro compounds can occur as follow:

$$Org - NO_2 \xrightarrow{hv} Org + HONO_{(g)} \quad \textbf{(R8)}$$

467 Hence, the obtained results from this study and the available literature suggest that the
468 HONO formation might result from a photodegradation of nitro-compounds and nitrogen-
469 containing compounds formed in the film, and/or from the photolysis of nitrate/nitric acid in
470 the presence of molds extract as organic compounds on the surfaces.

3.5. Implications for indoor air quality

In order to determine the concentration of HONO resulting from irradiated indoor surfaces contaminated with molds, the indoor concentration of HONO was estimated following the equation given by Willem et al.[73]:

$$\frac{d[HONO]}{dt} = \frac{E_{HONO} \times S}{V} - N_h[HONO] - J_{HONO}[HONO] \quad \textbf{(Eq. 3)}$$

where E_{HONO} is the emission rate of HONO in µg m^{-2} h^{-1}, S is the surface area of the room contaminated by molds (m^2), V is the room volume (m^3), N_h is the air exchange rate (h^{-1}) and J_{HONO} is the photolysis rate of indoor HONO. It is noteworthy mentioning that the loss on surfaces was already taken into account in the measured HONO concentration.

As the HONO outdoor levels are usually lower than indoor levels, it was assumed that there is no influence of outdoor concentration of HONO on the indoor concentration for this simulation.[74] The steady-state HONO concentration can be then simplified as:

$$[HONO] = \frac{E_{HONO} \times S}{V \times (J_{HONO} + N_h)} \quad \textbf{(Eq. 4)}$$

For indoor relevant relative humidity (RH = 45%), with an air exchange rate of 0.5 h^{-1} [73]and a photolysis rate of HONO equal to 0.25 h^{-1} [3,27] and considering a standard living room (S= 20 m^2, V =50 m^3) with a mold damaged surface of 0.25 m^2 and a nitrate concentration of 0.04M, the resulting HONO concentration from these surfaces is of the order of 60 ppt.

Moreover, the UV fraction of sunlight penetrating in indoor spaces ranges from 330 up to 400 nm depending on the location, time of the year, room orientation as well as the size and type of the glass window.[75] Additionally, Liu et al.[37] have shown high HONO yields during the irradiation period of the glass windows in the kitchen. Hence, the wavelength of the LED lamp used in this study corresponds to the lowest possible wavelength encountered indoor. Likewise, the corresponding photon flux is of 3.8×10^{12} photons $cm^{-2}s^{-1}$, which is lower than the direct

indoor UV actinic flux (with windows closed) measured by Gandolfo et al. (i.e., 10^{14} photons $cm^{-2}s^{-1}$) but significantly higher than the one in the shadows (i.e., 10^{10} photons $cm^{-2}s^{-1}$). Nevertheless, our experimental conditions can be somehow representative of realistic indoor conditions during sunny periods. Thus, for future studies, it will be interesting to evaluate the influence of different type of indoor light sources with different intensities on the HONO yields from different surfaces and mainly those covered by microbial species. This will help improving the model used to accurately predict the HONO concentrations values under different light intensities.

Finally, mold growth is especially found in damp dwellings with high relative humidity (>70%). In fact, sick buildings infested with visible molds, present a wide contaminated surface area compared to the one used in our calculation and have usually a low ventilation rate. For example, if the mold damaged surface is 25 m^2, and for the same nitrate concentration of 0.04M, the resulting HONO concentration in the gas phase will be around 6 ppb. Hence, indoor surfaces covered with molds can be a non-negligible source of HONO mainly in sick buildings exhibiting large, contaminated areas, alongside high relative humidity, and low ventilation rates. Typical indoor levels are of the order of few ppbs.[28,29,32] These levels could significantly be affected by surface chemistry as it was previously demonstrated for various indoor surfaces[29,32,76] and for microbial indoor surface in the present work.

4. Conclusions

In this study, we show that *Aspergillus niger*, a common indoor mold, can react on surfaces and produce a complex mixture of adsorbed products that initiate photochemistry indoors. These microbial species lead to the formation of VOCs and enhances HONO production under various indoor conditions including light irradiation, relative humidity and KNO_3 concentration. As microbial species are often found in areas with high relative humidity, the resulting HONO concentrations become significant. Hence, this work allows the recognition of

517 microbials species *(Aspergillus niger)* as a new indoor HONO source. This will definitely shed
518 a new light on the role of molds grown in sick dwellings in affecting the indoor air chemistry
519 and quality.

520 ## Acknowledgments

521 This work was supported by the Alfred P. Sloan Foundation under its Chemistry of Indoor
522 Environments program.

523 ## References

524 1. Park SS, Hong JH, Lee JH, Kim YJ, Cho SY, Kim SJ. Investigation of nitrous acid
525 concentration in an indoor environment using an in-situ monitoring system. *Atmos*
526 *Environ*. 2008;42:6586–6596.
527 2. Gandolfo A, Marque S, Temime-Roussel B, et al. Unexpectedly High Levels of Organic
528 Compounds Released by Indoor Photocatalytic Paints. *Environ Sci Technol*.
529 2018;52:11328–11337.
530 3. Zhou S, Young CJ, Vandenboer TC, Kowal SF, Kahan TF. Time-Resolved
531 Measurements of Nitric Oxide, Nitrogen Dioxide, and Nitrous Acid in an Occupied New
532 York Home. *Environ Sci Technol*. 2018;52:8355–8364.
533 4. Mendez M, Amedro D, Blond N, et al. Identification of the major HOx radical pathways
534 in an indoor air environment. *Indoor Air*. 2017;27:434–442.
535 5. Manuja A, Ritchie J, Buch K, et al. Total surface area in indoor environments. *Environ*
536 *Sci Process Impacts*. 2019;21:1384–1392.
537 6. Wainman T, Weschler CJ, Lioy PJ, Zhang J. Effects of surface type and relative humidity
538 on the production and concentration of nitrous acid in a model indoor environment.
539 *Environ Sci Technol*. 2001;35:2200–2206.
540 7. Schwartz-Narbonne H, Jones SH, Donaldson DJ. Indoor lighting releases gas phase
541 nitrogen oxides from indoor painted surfaces. *Environ Sci Technol Lett*. 2019;6:92–97.
542 8. Weschler CJ, Carslaw N. Indoor Chemistry. *Environ Sci Technol*. 2018;52:2419–2428.
543 9. Schwartz-Narbonne H, Donaldson DJ. Water uptake by indoor surface films. *Sci Rep*.
544 2019;9:11089.
545 10. Nazaroff WW, Goldstein AH. Indoor chemistry: research opportunities and challenges.
546 *Indoor Air*. 2015;25:357–361.
547 11. Farmer DK. Analytical challenges and opportunities for indoor air chemistry field
548 studies. *Anal Chem*. 2019;91:3761–3767.
549 12. Brown SK, Sim MR, Abramson MJ, Gray CN. Concentrations of Volatile Organic
550 Compounds in Indoor Air – A Review. *Indoor Air*. 1994;4:123–134.
551 13. Lee SC, Li WM, Ao CH. Investigation of indoor air quality at residential homes in Hong
552 Kong - Case study. *Atmos Environ*. 2002;36:225–237.
553 14. Uhde E, Salthammer T. Impact of reaction products from building materials and
554 furnishings on indoor air quality-A review of recent advances in indoor chemistry. *Atmos*
555 *Environ*. 2007;41:3111–3128.
556 15. Subramaniam M. Comparative study on indoor fungi growth incorporated with different
557 antifungal and wall finishings. 2017.
558 16. Polizzi V, Adams A, De Saeger S, Van Peteghem C, Moretti A, De Kimpe N. Influence

of various growth parameters on fungal growth and volatile metabolite production by indoor molds. *Sci Total Environ*. 2012;414:277–286.
17. Matysik S, Herbarth O, Mueller A. Determination of volatile metabolites originating from mould growth on wall paper and synthetic media. *J Microbiol Methods*. 2008;75:182–187.
18. Reboux G, Bellanger AP, Roussel S, et al. Indoor mold concentration in Eastern France. *Indoor Air*. 2009;19:446–453.
19. Priegnitz B, Wargenau A, Brandt U, et al. The role of initial spore adhesion in pellet and biofilm formation in Aspergillus niger. *Fungal Genet Biol*. 2012;49:30–38.
20. Korpi A, Pasanen AL, Pasanen P. Volatile Compounds Originating from Mixed Microbial cultures on building materials under various humidity conditions. *Appl Environ Microbiol*. 1998;64:2914–2919.
21. Korpi A, Järnberg J, Pasanen AL. Microbial volatile organic compounds. *Crit Rev Toxicol*. 2009;39:139–193.
22. Lorenz W, Diederich T, Conrad M. Practical experiences with MVOC as an indicator for microbial growth. *Proc Indoor Air 2002*. 2002:341–346.
23. Kalalian C, Abis L, Depoorter A, Lunardelli B, Perrier S, George C. Influence of indoor chemistry on the emission of mVOCs from Aspergillus niger molds. *Sci Total Environ*. 2020;741:140148.
24. Velazquez S, Griffiths W, Dietz L, et al. From one species to another: A review on the interaction between chemistry and microbiology in relation to cleaning in the built environment. *Indoor Air*. 2019;29:880–894.
25. Xie Z, Li Y, Lu R, et al. Characteristics of total airborne microbes at various air quality levels. *J Aerosol Sci*. 2018;116:57–65.
26. Guo J, Xiong Y, Kang T, Zhu H, Yang Q, Qin C. Effect of formaldehyde exposure on bacterial communities in simulating indoor environments. *Sci Rep*. 2021;11:20575.
27. Alvarez EG, Amedro D, Afif C, et al. Unexpectedly high indoor hydroxyl radical concentrations associated with nitrous acid. *Proc Natl Acad Sci U S A*. 2013;110:13294–13299.
28. Bartolomei V, Sörgel M, Gligorovski S, et al. Formation of indoor nitrous acid (HONO) by light-induced NO2 heterogeneous reactions with white wall paint. *Environ Sci Pollut Res*. 2014;21:9259–9269.
29. Gómez Alvarez E, Sörgel M, Gligorovski S, et al. Light-induced nitrous acid (HONO) production from NO2heterogeneous reactions on household chemicals. *Atmos Environ*. 2014;95:391–399.
30. George C, Ammann M, D'Anna B, Donaldson DJ, Nizkorodov SA. Heterogeneous Photochemistry in the Atmosphere. *Chem Rev*. 2015.
31. Ammar R, Monge ME, George C, D'Anna B. Photoenhanced NO2 loss on simulated urban grime. *ChemPhysChem*. 2010;11:3956–3961.
32. Depoorter A, Kalalian C, Emmelin C, Lorentz C, George C. Indoor heterogeneous photochemistry of furfural drives emissions of nitrous acid. *Indoor Air*. 2020:1–11.
33. Wang X, Dalton EZ, Payne ZC, et al. Superoxide and Nitrous Acid Production from Nitrate Photolysis Is Enhanced by Dissolved Aliphatic Organic Matter. *Environ Sci Technol Lett*. 2020;8:53–58.
34. Bhattarai HR, Virkajärvi P, Yli-Pirilä P, Maljanen M. Emissions of atmospherically important nitrous acid (HONO) gas from northern grassland soil increases in the presence of nitrite (NO2−). *Agric Ecosyst Environ*. 2018;256:194–199.
35. Morrison G. Recent Advances in Indoor Chemistry. *Curr Sustain Energy Reports*. 2015;2:33–40.
36. Arata C, Zarzana KJ, Misztal PK, et al. Measurement of NO3 and N2 O5 in a Residential

609 Kitchen. *Environ Sci Technol lett*. 2018;5:595–599.
610 37. Liu J, Deng H, Lakey PSJ, et al. Unexpectedly High Indoor HONO Concentrations
611 Associated with Photochemical NO2Transformation on Glass Windows. *Environ Sci*
612 *Technol*. 2020;54:15680–15688.
613 38. Weschler CJ, Nazaroff WW. *Growth of Organic Films on Indoor Surfaces*. Vol 27.;
614 2017.
615 39. Yang W, Han C, Yang H, Xue X. Significant HONO formation by the photolysis of
616 nitrates in the presence of humic acids. *Environ Pollut*. 2018;243:679–686.
617 40. Sunesson AL, Vaes WHJ, Nilsson CA, Blomquist G, Andersson B, Carlson R.
618 Identification of volatile metabolites from five fungal species cultivated on two media.
619 *Appl Environ Microbiol*. 1995;61:2911–2918.
620 41. Wang X, Hayeck N, Brüggemann M, et al. Chemical Characteristics of Organic Aerosols
621 in Shanghai: A Study by Ultrahigh-Performance Liquid Chromatography Coupled With
622 Orbitrap Mass Spectrometry. *J Geophys Res Atmos*. 2017;122:11,703-11,722.
623 42. Wang X, Hayeck N, Brüggemann M, et al. Chemical Characteristics and Brown Carbon
624 Chromophores of Atmospheric Organic Aerosols Over the Yangtze River Channel: A
625 Cruise Campaign. *J Geophys Res Atmos*. 2020;125:1–13.
626 43. Lin P, Rincon AG, Kalberer M, Yu JZ. Elemental composition of HULIS in the Pearl
627 River Delta Region, China: Results inferred from positive and negative electrospray high
628 resolution mass spectrometric data. *Environ Sci Technol*. 2012;46:7454–7462.
629 44. Yassine MM, Harir M, Dabek-Zlotorzynska E, Schmitt-Kopplin P. Structural
630 characterization of organic aerosol using Fourier transform ion cyclotron resonance mass
631 spectrometry: aromaticity equivalent approach. *Rapid Commun Mass Spectrom*.
632 2014;28:2445–2454.
633 45. Uniprot. Swiss-Prot database. https://www.uniprot.org/.
634 46. metabolomics workbench. https://www.metabolomicsworkbench.org/.
635 47. RSCB. protein data bank. https://www.rcsb.org/.
636 48. Heland J, Kleffmann J, Kurtenbach R, Wiesen P. A new instrument to measure gaseous
637 nitrous acid (HONO) in the atmosphere. *Environ Sci Technol*. 2001;35:3207–3212.
638 49. Villena G, Bejan I, Kurtenbach R, Wiesen P, Kleffmann J. Development of a new Long
639 Path Absorption Photometer (LOPAP) instrument for the sensitive detection of NO2 in
640 the atmosphere. *Atmos Meas Tech*. 2011;4:1663–1676.
641 50. Cappellin L, Karl T, Probst M, et al. On quantitative determination of volatile organic
642 compound concentrations using proton transfer reaction time-of-flight mass
643 spectrometry. *Environ Sci Technol*. 2012;46:2283–2290.
644 51. de Gouw JA, Goldan PD, Warneke C, et al. Validation of proton transfer reaction-mass
645 spectrometry (PTR-MS) measurements of gas-phase organic compounds in the
646 atmosphere during the New England Air Quality Study (NEAQS) in 2002. *J Geophys*
647 *Res Atmos*. 2003;108:1–18.
648 52. Lindinger W, Hansel A, Jordan A. On-line monitoring of volatile organic compounds at
649 pptv levels by means of Proton-Transfer-Reaction Mass Spectrometry (PTR-MS)
650 Medical applications, food control and environmental research. *Int J Mass Spectrom Ion*
651 *Process*. 1998;173:191–241.
652 53. Cappellin L, Biasioli F, Granitto PM, et al. On data analysis in PTR-TOF-MS: From raw
653 spectra to data mining. *Sensors Actuators, B Chem*. 2011;155:183–190.
654 54. Moularat S, Robine E, Ramalho O, Oturan MA. Detection of fungal development in a
655 closed environment through the identification of specific VOC: Demonstration of a
656 specific VOC fingerprint for fungal development. *Sci Total Environ*. 2008;407:139–146.
657 55. Sager EE, Byers FC. Spectral absorbance of some aqueous solutions in the range 10-
658 degrees to 40-degrees-C. *J Res Natl Bur Stand (1934)*. 1957;58:33.

56. Ye C, Zhang N, Gao H, Zhou X. Matrix effect on surface-catalyzed photolysis of nitric acid. *Sci Rep*. 2019;9:1–10.
57. Franze T, Weller MG, Niessner R, Pöschl U. Protein nitration by polluted air. *Environ Sci Technol*. 2005;39:1673–1678.
58. Meusel H, Elshorbany Y, Kuhn U, et al. Light-induced protein nitration and degradation with HONO emission. *Atmos Chem Phys*. 2017;17:11819–11833.
59. Ghiani A, Bruschi M, Citterio S, et al. Nitration of pollen aeroallergens by nitrate ion in conditions simulating the liquid water phase of atmospheric particles. *Sci Total Environ*. 2016;573:1589–1597.
60. Vione D, Maurino V, Minero C, Lucchiari M, Pelizzetti E. Nitration and hydroxylation of benzene in the presence of nitrite/nitrous acid in aqueous solution. *Chemosphere*. 2004;56:1049–1059.
61. Krappmann S, Braus GH. Nitrogen metabolism of Aspergillus and its role in pathogenicity. *Med Mycol*. 2005;43.
62. Cánovas D, Marcos JF, Marcos AT, Strauss J. Nitric oxide in fungi: is there NO light at the end of the tunnel? *Curr Genet*. 2016;62:513–518.
63. McLean S, Bowman LAH, Sanguinetti G, Read RC, Poole RK. Peroxynitrite toxicity in Escherichia coli K12 elicits expression of oxidative stress responses and protein nitration and nitrosylation. *J Biol Chem*. 2010;285:20724–20731.
64. Warris A, Ballou ER. Oxidative responses and fungal infection biology. *Semin Cell Dev Biol*. 2019;89:34–46.
65. Yang H, Zhang Y, Pöschl U. Quantification of nitrotyrosine in nitrated proteins. *Anal Bioanal Chem*. 2010;397:879–886.
66. Szabó C, Ischiropoulos H, Radi R. Peroxynitrite: Biochemistry, pathophysiology and development of therapeutics. *Nat Rev Drug Discov*. 2007;6:662–680.
67. Freney EJ, Martin ST, Buseck PR. Deliquescence and efflorescence of potassium salts relevant to biomass-burning aerosol particles. *Aerosol Sci Technol*. 2009;43:799–807.
68. Zhou X, Gao H, He Y, et al. Nitric acid photolysis on surfaces in low-NOx environments: Significant atmospheric implications. *Geophys Res Lett*. 2003;30:10–13.
69. Finlayson-Pitts BJ, Wingen LM, Sumner AL, Syomin D, Ramazan KA. The heterogeneous hydrolysis of NO2 in laboratory systems and in outdoor and indoor atmospheres: An integrated mechanism. *Phys Chem Chem Phys*. 2003;5:223–242.
70. Ma J, Liu Y, Han C, Ma Q, Liu C, He H. Review of heterogeneous photochemical reactions of NOy on aerosol - A possible daytime source of nitrous acid (HONO) in the atmosphere. *J Environ Sci (China)*. 2013;25:326–334.
71. Ray AC, Eakin RE. Studies on the Biosynthesis of Aspergillin byAspergillus niger. *Appl Microbiol*. 1975;30:909–915.
72. Stemmler K, Ammann M, Donders C, Kleffmann J, George C. Photosensitized reduction of nitrogen dioxide on humic acid as a source of nitrous acid. *Nature*. 2006;440:195–198.
73. Willem H, Hult EL, Hotchi T, Russell L, Maddalena RL, Singer BC. *Ventilation Control of Volatile Organic Compounds in New U . S . Homes : Results of a Controlled Field Study in Nine Residential Units*.; 2013.
74. Lee K, Xue J, Geyh AS, et al. Nitrous acid, nitrogen dioxide, and ozone concentrations in residential environments. *Environ Health Perspect*. 2002;110:145–149.
75. Gandolfo A, Gligorovski V, Bartolomei V, et al. Spectrally resolved actinic flux and photolysis frequencies of key species within an indoor environment. *Build Environ*. 2016;109:50–57.
76. Wang C, Collins DB, Arata C, et al. Surface reservoirs dominate dynamic gas-surface partitioning of many indoor air constituents. *Sci Adv*. 2020;6:1–12.